Decadal Variability in Spring Sea Ice Concentration Linked to Summer Temperature and NDVI on the Yukon–Kuskokwim Delta

AMY S. HENDRICKS,[a] UMA S. BHATT,[a] GERALD V. FROST,[b] DONALD A. WALKER,[c] PETER A. BIENIEK,[d] MARTHA K. RAYNOLDS,[c] RICK T. LADER,[d] HOWARD E. EPSTEIN,[e] JORGE E. PINZON,[f] COMPTON J. TUCKER,[f] AND JOSEFINO C. COMISO[g]

[a] *Department of Atmospheric Sciences, College of Natural Science and Mathematics, Geophysical Institute, University of Alaska Fairbanks, Fairbanks, Alaska*
[b] *ABR, Inc.–Environmental Research and Services, Fairbanks, Alaska*
[c] *Institute of Arctic Biology, University of Alaska Fairbanks, Fairbanks, Alaska*
[d] *International Arctic Research Center, University of Alaska Fairbanks, Fairbanks, Alaska*
[e] *Department of Environmental Sciences, University of Virginia, Charlottesville, Virginia*
[f] *Biospheric Science Branch, NASA Goddard Space Flight Center, Greenbelt, Maryland*
[g] *Cryospheric Sciences Branch, NASA Goddard Space Flight Center, Greenbelt, Maryland*

(Manuscript received 20 February 2023, in final form 20 September 2023, accepted 25 September 2023)

ABSTRACT: Rapidly warming temperatures in the Arctic are driving increasing tundra vegetation productivity, evidenced in both the satellite derived normalized difference vegetation index (NDVI) imagery and field studies. These trends, however, are not uniformly positive across the circumpolar Arctic. One notable region of negative linear NDVI trends that have persisted over the last 15 years is southwest Alaska's Yukon–Kuskokwim Delta (YKD). Negative NDVI trends in the YKD region appear inconsistent with our understanding since tundra vegetation is temperature-limited and air temperatures have increased on the YKD. Analysis over a 40-yr record from 1982 to 2021 reveals distinct decadal variability in the NDVI time series, which continues to produce negative linear trends. Similar decadal variability is also evident in summer warmth and 100-km coastal zone spring sea ice concentrations. This suggests that decadal climate variations can dominate the trends of NDVI through their influence on the drivers of tundra vegetation, namely, coastal sea ice concentrations and summer warmth. The relationships among sea ice, summer warmth, and NDVI have changed over the 40-yr record. Seasonality analysis since 1982 shows declining sea ice concentration in spring is followed by trends of increasing temperatures, but weakly declining NDVI during the growing season. An additional key finding is that since early 2010s, the relationships between sea ice concentration and summer warmth, and sea ice concentration and NDVI have strengthened, while the relationship between NDVI and summer warmth has weakened, indicating that temperature may no longer be the primary limiting factor for Arctic tundra vegetation on the YKD.

SIGNIFICANCE STATEMENT: This paper addresses a curiosity of regional Arctic climate change, which is that despite increasing temperatures, spatially and temporally declining trends of vegetation productivity on the Yukon–Kuskokwim Delta appear in satellite data. This study bridges our understanding of Arctic climate relationships at varying scales and informs questions about how these relationships may change in the future.

KEYWORDS: Atmosphere–land interaction; Atmosphere–ocean interaction; Climate variability

1. Introduction

A defining feature of Arctic climate change is the striking response of tundra vegetation productivity to increasing summer temperatures, a phenomenon known as the "greening of the Arctic" (Myneni et al. 1997; Jia et al. 2003). Remotely sensed trends of vegetation productivity are derived from satellite sensors such as the Advanced Very High Resolution Radiometer (AVHRR); red and near-infrared reflectance are used to calculate the normalized difference vegetation index (NDVI), which is a good proxy for vegetation productivity (Tucker et al. 2005; Pinzon and Tucker 2014). NDVI displays a strong positive relationship with land surface temperature patterns (Raynolds et al. 2008), and early analysis of AVHRR NDVI revealed a positive trend of plant growth at high latitudes from 1982 to 1991 (Myneni et al. 1997).

Arctic tundra plants are temperature limited (Walker et al. 2005; Chapin et al. 1995) during relatively short growing seasons when sunlight is available for photosynthesis. Favorably for Arctic tundra plants, temperatures in the Arctic are rising at accelerated rates relative to the global average rate (Ballinger et al. 2022) because of a defining mechanism in the Arctic climate system known as Arctic amplification (Screen and Simmonds 2010). Increasing global greenhouse gas emissions are driving the rapid decline and degradation of Arctic sea

Corresponding author: Amy Hendricks, ashendricks@alaska.edu

Earth Interactions is published jointly by the American Meteorological Society, the American Geophysical Union, and the Association of American Geographers.

DOI: 10.1175/EI-D-23-0002.1 e230002

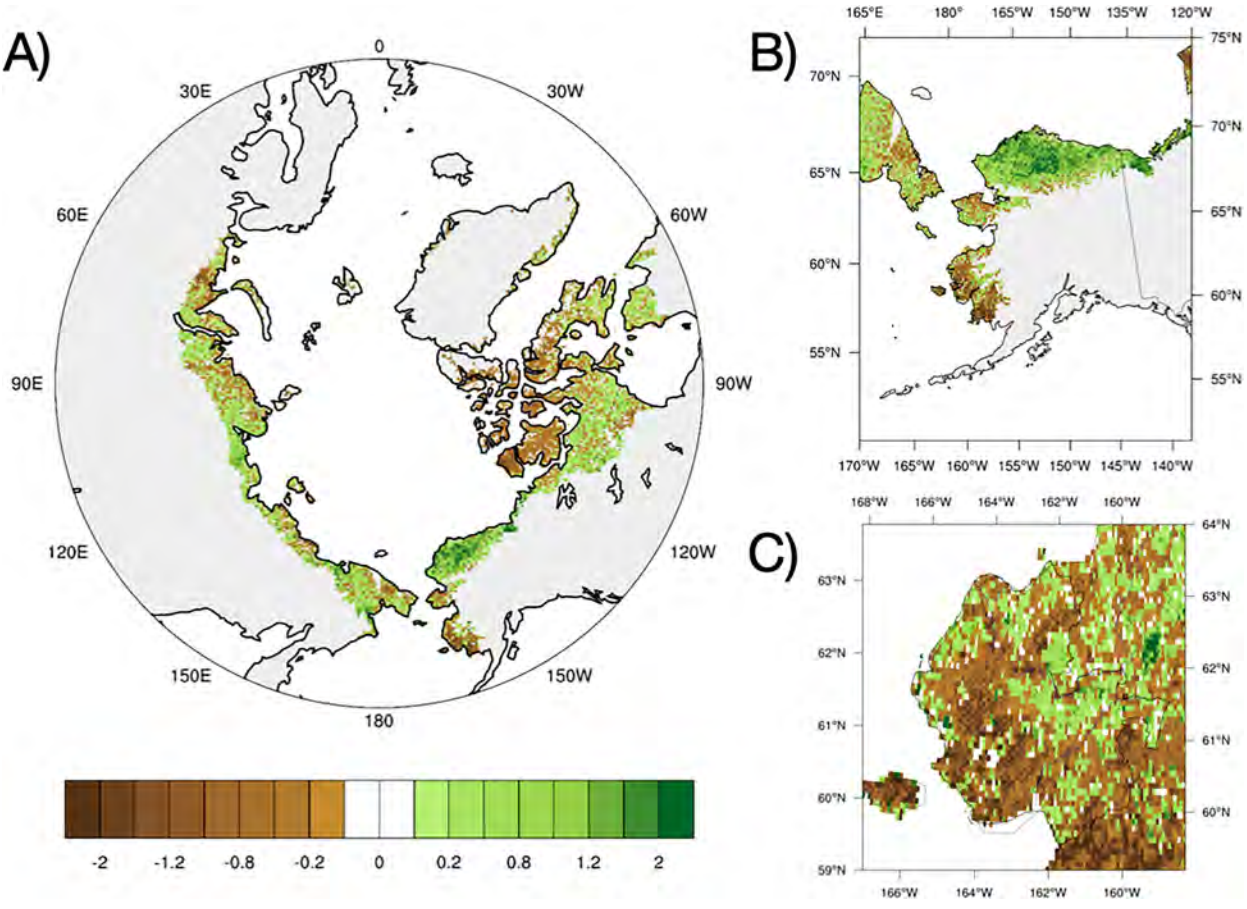

FIG. 1. Trends of Arctic tundra AVHRR satellite-derived time integrated NDVI (TI-NDVI; unitless) from 1982 to 2021: (a) The circumpolar Arctic overall displays an increasing trend in NDVI (green). In this polar projection, Alaska and the YKD are in the bottom right. (b) The YKD is a region of notable declining TI-NDVI (brown). (c) TI-NDVI trends in the YKD region are not uniformly declining, with some areas of increasing trends. Units are TI-NDVI (unitless) over 40 years.

ice (Stroeve et al. 2007), which is an essential component of the sea ice–albedo feedback mechanism, where bright sea ice reflects solar radiation during spring and summer months when the sun returns. Diminishing multiyear sea ice and poor conditions for sea ice formation have given way to increasing open water during the spring, and as a result, larger areas of darker ocean surface are open to absorb incoming solar radiation (Holland and Bitz 2003). The higher heat capacity of the sea surface water helps to warm the air and land surface during the subsequent growing season (Bhatt et al. 2017), leading to increasing tundra phytomass (Circumpolar Arctic Vegetation Map Team 2003; Walker et al. 2003). Proximity to cooler Arctic seas moderates summer temperatures, and as 80% of nonalpine tundra is located within 100 km of a coastline, Arctic tundra is essentially a maritime biome (Walker et al. 2003). The linkages between spring sea ice concentration, cumulative summer warmth, and Arctic tundra productivity were first documented in 2010, and it was noted specifically that the annual timing of the 50% spring sea ice concentration is especially important for coastal and near-coastal tundra regions (Bhatt et al. 2010).

Subsequent decades of research continued to witness increasing NDVI trends in the Arctic tundra biome (Bieniek et al. 2015; Park et al. 2016; Box et al. 2019; Berner et al. 2020); however, studies have also revealed that patterns of Arctic tundra responses to warmer growing seasons are not uniform (Myers-Smith et al. 2020; Goetz et al. 2010), and more recent correlations between NDVI and summer temperature have weakened (Bhatt et al. 2021). Circumpolar AVHRR NDVI trends for 1982–2021 are shown in Fig. 1a; the figure shows time-integrated NDVI (TI-NDVI), which is the sum of biweekly NDVI values and incorporates the entirety of a growing season, making it a good indicator for investigating links to climate drivers. While overall TI-NDVI trends in the Arctic are positive, several regions of declining trends have persisted despite warming temperatures. Negative NDVI trends have also appeared over Norway (excluding Svalbard), Sweden and Finland north of the Arctic Circle, which have been attributed to winter warming and extreme events such as rain on snow, early spring thaws and late frosts, and pest outbreaks (Bjerke et al. 2014; Bokhorst et al. 2009). Landform changes, such as disturbances from permafrost degradation

(Lara et al. 2018; Jorgenson et al. 2018), wildfires (Frost et al. 2020), and summer drought (Bjerke et al. 2014) are also known to drive negative NDVI trends on more localized scales. The local responses and nonuniform spatial patterns in remotely sensed climate data highlight the importance of regional studies to better understand the complex drivers of vegetation changes in the evolving Arctic.

Southwest Alaska's expansive Yukon–Kuskokwim Delta (YKD) stands out as a notable region of widespread NDVI decline in the extensive 40-yr AVHRR record for 1982–2021 (Figs. 1b,c). The negative trends were first noted in 2008 (Verbyla 2008) and have continued to intrigue researchers, since temperature is the key limiting factor for tundra productivity at large spatial scales, and average monthly summer temperatures display positive trends in this region (Frost et al. 2021). Early AVHRR NDVI trends on the YKD were consistent with greening trends across the Arctic; however, trends on the YKD reversed after 1998 (Frost et al. 2021), and the widespread extent of negative NDVI trends on the YKD (Fig. 1c) suggests large-scale climate drivers at work. The Bering Sea region is particularly subject to decadal and multidecadal climate variability, derived from the Pacific decadal oscillation and other modes of climate variability (Yang et al. 2020), which likely plays a role in the long-term temperature trends on the YKD.

This paper offers an explanation behind long-term NDVI trends on the YKD by examining trends and variability of climate drivers at the regional scale. Now that the AVHRR record extends to four decades, analysis over the 1982–2021 period reveals insights into the processes operating over decadal time scales. This study was guided by two main questions:

1) What are long-term variations and trends of NDVI on the YKD?
2) Can regional climate variations provide insight into the variability and trends of NDVI on the YKD?

The data and methods in section 2 introduce the study region, data resources and metadata, and methodology. Results of the analysis are presented in section 3, followed by a discussion highlighting insights into the connections among sea ice concentration, summer warmth, and NDVI variability on the YKD in section 4. The conclusions are in section 5.

2. Methods

a. YKD study region

The YKD study area for this project (Fig. 1c) is in southwest Alaska along the Bering Sea coast (59.9°–63.5°N, 158°–166°W) and includes the region bounded by the Yukon Delta National Wildlife Refuge and the YKD ecoregion, totaling approximately 96 178 km^2 (Frost et al. 2021; Nowacki et al. 2003). Encompassing the southern half of Alaska's western climate division (Bieniek et al. 2012), the YKD experiences relatively warm winter air temperatures, with a December–February long-term mean of −9°C over the period 1960–2020 for the Alaska west coast climate division (NCEI 2022). The region experiences frequent winter thaw and rain-on-snow events (Bieniek et al. 2018), and coastal sea ice with large interannual variability. The YKD represents a southern endmember of the Arctic tundra biome (Frost et al. 2021). As detailed in Fig. A1 and Table A1 of the appendix, six physiographic regions describe the varied YKD landscape: coastal, coastal plain, deltaic, lowland, riverine, and upland (Frost et al. 2021). The YKD is highly biologically diverse, hosting globally significant migratory waterfowl breeding grounds (Gill and Handel 1990), and supporting Yup'ik peoples, who have traditionally relied on the land for subsistence resources for thousands of years (Fienup-Riordan 1999; Klein 1966).

b. Datasets

1) NDVI

Remotely sensed biweekly composited NDVI for 1982–2021 is derived from a collection of AVHRR sensors aboard National Oceanic and Atmospheric Administration (NOAA) satellites (Pinzon et al. 2023). As part of the National Aeronautics and Space Administration (NASA) Global Inventory Modeling and Monitoring System (GIMMS), Sea-viewing Wide Field-of-view Sensor data are used for calibrating among the collection of sensors (Pinzon and Tucker 2014). The 8-km-resolution NDVI3g V1.2 dataset includes corrections for discontinuities done in earlier versions of the GIMMS NDVI dataset north of 72°N, which permitted the first comprehensive analysis of NDVI trends in the High Arctic (Bhatt et al. 2010). Two representations of NDVI are analyzed at 1/12° spatial resolution: 1) MaxNDVI is the highest biweekly value observed over a growing season, representing peak photosynthetic capacity (Tucker 1977; Myneni et al. 1997), and 2) TI-NDVI is the total sum of biweekly NDVI values for May through September, matching ground observations of senescence, that exceed a threshold value of 0.05. The low threshold value allows for examining changes during early and late growing season, especially during the snowmelt period during which rapid green-up occurs (Gamon et al. 2013). Over the more southerly tundra region, transient snow and snow-free periods during winter months expose dormant plants, keeping biweekly NDVI at or above 0.2, whereas regions with continuous snow cover can display NDVI near zero during the cold season. TI-NDVI incorporates the entirety of the growing season, making it a better indicator for investigating climate drivers when compared with MaxNDVI (Bhatt et al. 2010). In the TI-NDVI calculation, if biweekly values are missing at a given pixel, then they are filled by the mean value for that biweekly period over the 1982–2021 period using all data points that are available.

2) SEA ICE CONCENTRATION AND OPEN WATER

Spring sea ice concentration for 1982–2021 is analyzed using data from the Special Sensor Microwave Imager (Comiso and Nishio 2008), archived at the NASA Distributed Active Archive Center hosted by National Snow and Ice Data Center (https://nsidc.org/data/nsidc-0079/versions/3). Spring sea ice concentration values are calculated by first determining a climatological 3-week period during which sea ice concentrations

reach 50%. The value used is a date centered in the 3-week period. Spatial concentrations are determined on a 25-km-resolution grid for the east Bering region within 100-km of the coastline and south of 63.5°N. As the timing of 50% spring sea ice concentration exhibits high interannual and spatial variability, this particular methodology has been effective in capturing the relationship between sea ice concentration and TI-NDVI (Bhatt et al. 2010, 2021). The inverse of sea ice concentration, open water is the percentage of a grid cell not covered by sea ice, and summer open water is the seasonal average of weekly open water from May through August.

3) Summer warmth index and temperature

Summer warmth index (SWI) is the accumulated sum of monthly average temperature above freezing between April and September (unit: °C months). SWI is calculated from 2-m air temperature provided by the fifth major global reanalysis produced by ECMWF (ERA5) dataset (Hersbach et al. 2020). ERA5 data were downloaded from the Climate Data Store (https://cds.climate.copernicus.eu/), available for free with an account. Data were downloaded on a 0.25° × 0.25° grid, and bilinearly interpolated to 1/12° resolution by employing NCAR Command Language functions that utilize Earth System Modeling Framework software. For temperature in Alaska, the ERA5 is shown to minimize discontinuities in station observations (White et al. 2021) and shows similar variability and trends when compared with AVHRR surface temperatures for the YKD (Frost et al. 2021).

4) Analysis methods

This study presents the least squares method to calculate trends, allowing a direct comparison with previous research that displayed negative NDVI trends on the YKD. In addition, since the key finding of this paper concerns decadal variations in climate drivers, the utility of Theil–Sen is unclear for time series with low-frequency variations, which are different from outliers. Linear trends were calculated using the least squares fit method for the full time series over the 1982–2021 period, for individual grid cells, and a spatial average for the YKD study region and 100-km coastal buffer strip. Trends were also calculated using the nonparametric Theil–Sen method and the results were not notably different than least squares fit, consistent with previous findings (Bhatt et al. 2021). Pearson's correlation coefficients were calculated on linearly detrended time series, and significance was tested using the Student's t test, which is a similar method to previous research in which interannual correlations in Arctic tundra NDVI research did not shown strong temporal autocorrelation (1-yr lag) (Reichle et al. 2018). Linear detrending was calculated using the least squares fit method, and significance was assessed using an f test. Multilinear regression was conducted on normalized time series. Effective degrees of freedom to evaluate statistical significance were calculated using lag-1 autocorrelations (Santer et al. 2000), and confidence is displayed in the graphics for the 95% or greater level.

3. Results

The first major result of this study is the clear long-term decadal variability in the 40-yr AVHRR records for both MaxNDVI and TI-NDVI on the YKD (Fig. 2a). Both TI-NDVI and MaxNDVI show increasing trends early in the record, peaking during the 1990s, followed by a steady decline until around 2010. Since 2010 there has been a sharp rise in both TI-NDVI and biweekly NDVI until 2021. Long-term climatological averages for TI-NDVI and biweekly MaxNDVI are 5.42 and 0.71 (unitless), respectively. Both NDVI time series display substantial interannual variability in the YKD region (σ = 0.304 and 0.02, respectively), which has helped to obscure long-term NDVI trends in the previous research that used shorter study periods (e.g., Bhatt et al. 2017; Frost et al. 2021). Despite the extended length of data records to 40 years, TI-NDVI and MaxNDVI display negative albeit weak linear trends [-0.35 (40 yr)$^{-1}$ and 0.01 (40 yr)$^{-1}$, respectively] (Fig. 2a, dashed lines) for the 1982–2021 study period.

A second major finding is the notable long-term decadal coherence among NDVI, spring sea ice concentration, and SWI and the regional scale (Fig. 2b). The decadal-scale variations in TI-NDVI correspond clearly with the sea ice variability (note the reversed y axis) and associated SWI variability. Spring sea ice concentration displays a decreasing trend of -14.4% (40 yr)$^{-1}$, summer open water increased 3.7% (40 yr)$^{-1}$ (not shown), and summer warmth increased by 7.8°C months over the 40-yr study period. Since 2010, there has been a consistent decline in spring sea ice and an associated increase in summer warmth that corresponds to positive TI-NDVI trends. Strong increasing TI-NDVI trends since 2010 in the time series are also widespread over the study region, (Fig. 2c) and greatest in landscapes dominates by upland physiography (see Fig. A1 in the appendix). The low-frequency pattern of spring sea ice concentration and summer warmth variability on the YKD was first noted in 2021 (Frost et al. 2021); however, data for NDVI were not displayed with sea ice concentration and summer warmth, and the coherence among variables was not as clear as in Fig. 2b.

Despite coherent long-term decadal variability, relationships among spring sea ice concentration (SIC), TI-NDVI, and summer warmth have changed over time. This is explored further through linear correlation analysis between the variables (Table 1) and multilinear regression (Table 2) for the entire record (1982–2021), first half of the record (1982–2001), and second half of record (2002–21). Correlation analyses show the relationship between sea ice concentration and TI-NDVI strengthened over time, but the cubic detrended correlation showed little change. The relationship between SWI and TI-NDVI weakened from the first half to second half of the study period; however, the relationships showed little change in the cubic detrended time series (see Fig. A2 in the appendix). Multiple linear regression analysis supports the correlation analysis; absolute values of regression coefficients are similar for sea ice concentration and SWI on TI-NDVI for the entire study period (-0.29 and 0.24, respectively). However, when the full study period is split, SWI was a stronger driver of TI-NDVI in the early period than in the second half. Sea ice concentration shows a weakening driving effect of TI-NDVI over time. These

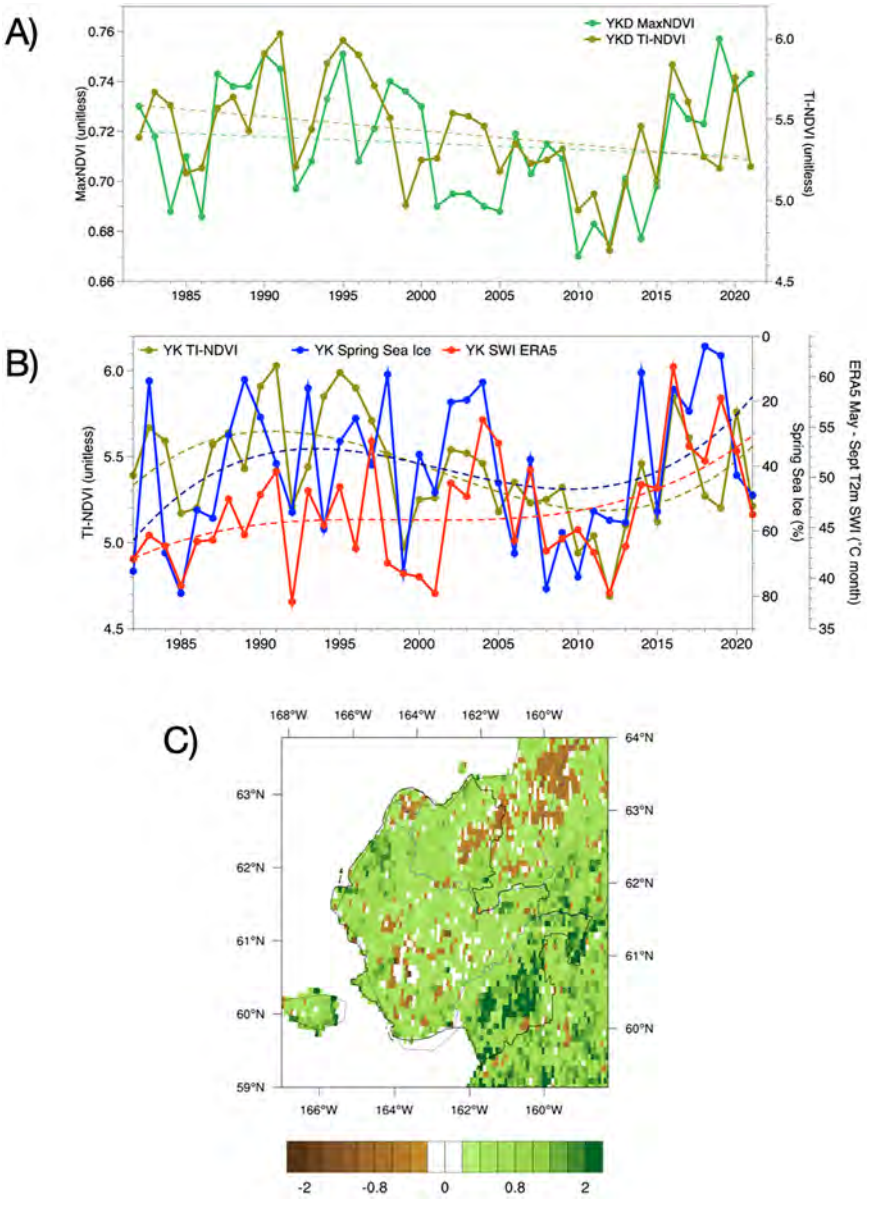

FIG. 2. (a) Annual time series of AVHRR MaxNDVI (green) and TI-NDVI (olive) show decadal variability, which results in a negative linear trend from 1982 to 2021 but with strong positive trends in the last decade. (b) Time series of TI-NDVI (olive), SWI (red), and 100-km coastal spring sea ice concentration (blue) show similar decadal variability, identified by the corresponding dashed cubic-fit lines. (c) Spatial TI-NDVI trend over the 2010–21 period highlights widespread positive trends in the YKD over the last decade. NDVI is unitless, SWI has units of degrees Celsius months, and sea ice concentration is in percent [note the reversed *y* axis for spring sea ice in (b)].

analyses suggests that temperature may no longer be the limiting factor for Arctic tundra vegetation, and that other drivers are increasing in importance.

Since TI-NDVI is a function of intraseasonal variations of biweekly NDVI, a seasonality examination is presented next to provide a more complete perspective. The seasonal climatology and trends of biweekly NDVI, monthly sea ice concentration, and monthly 2-m air temperature highlight the course of the seasonal cycle and how it is changing (Fig. 3). The regionally averaged YKD biweekly NDVI climatology rises quickly from 0.12 in early April to 0.43 by the second half of May and reaches a peak of 0.67 in the second half of July, after which it gradually decreases to a late September value of 0.47. Biweekly NDVI trends are weakly negative from June to the first half of September (Fig. 3a), and significantly negative for early May, late July, and early September. The

TABLE 1. Correlations for the full and partial study periods between SIC, SWI, and TI-NDVI for the YKD (boldface is 95% or greater confidence, and italics are 90% or greater confidence). Full time series correlations appear first, followed by detrended-from-cubic-fit correlations in parentheses.

Period		SWI	TI-NDVI
1982–2021	Sea ice	**−0.57 (−0.54)**	**−0.41 (−0.41)**
	SWI	—	**0.4 (0.61)**
1982–2001	Sea ice	*−0.40* (−0.33)	*−0.43* (*−0.38*)
	SWI	—	**0.71 (0.64)**
2002–21	Sea ice	**−0.74 (−0.70)**	**−0.52** (*−0.44*)
	SWI	—	**0.66 (0.60)**

TABLE 2. Multilinear regression coefficients on normalized time series for the full and partial study periods for sea ice concentration and SWI on TI-NDVI for the YKD (boldface is 95% or greater confidence, and italics are 90% or greater confidence).

Period	Sea ice	SWI
1982–2021	−0.29	0.24
1982–2001	−0.19	**0.82**
2002–21	0.01	**0.56**

notable NDVI trends in November may be attributed to changing snow cover and surface reflectance during a dynamic period, which is outside the season and scope of this study.

The spring sea ice concentration climatology in the 100-km coastal zone begins a seasonal melt and retreat, or break up, beginning in late March, and reaches the 50% concentration mark during the third week in April (Fig. 3b). The 100-km coastal area of the YKD is largely free of sea ice from June to October. Coastal spring sea ice concentration seasonality shows the largest declining trends of approximately 10% from mid-April into June for 1982–2021, although none of the trends are statistically significant. Growing-season 2-m air temperatures range from −3.3°C in April, to an average maximum of 12.4°C in July (Fig. 3c). Each month of the growing season is experiencing increasing temperatures, with the greatest increasing trends early in the growing season [4.0°C (40 yr)$^{-1}$ for April], with weaker positive trends during the peak of the growing season. The temperature trends are largest at the start and end of the growing season, corresponding to the timing of the early retreat and delayed advance of sea ice, respectively.

4. Discussion

a. *Changing influence of spring sea ice on tundra productivity*

Widespread declining NDVI trends across the YKD, first documented in 2008 (Verbyla 2008), motivated an investigation of climate variability and vegetation productivity at a regional scale over a 40-yr study period, which revealed corresponding low-frequency variability in spring sea ice concentration, summer warmth, and NDVI. Mechanisms previously considered include extended winter snow cover, vegetation dieback from winter thaw–freeze events, increased cloudiness, and insect infestations. While these factors may indeed influence the NDVI on interannual time scales, the overall low-frequency variations appear closely tied with coastal spring sea ice concentration. While long-term sea ice trends have been negative and temperature trends have been positive (Bhatt et al. 2021), an earlier regional view of trends revealed some indications of coherent decadal (Frost et al. 2021).

This low-frequency variability in GIMMS3g NDVI is not present in other Arctic tundra NDVI time series and has no known biological mechanism for low-frequency variability, so is likely associated with large-scale climate drivers. The low-frequency variations in the Bering Sea are not unique in the Arctic since sea ice in the Kara and Barents Seas is also influenced by decadal variability in the North Atlantic (Polyakov et al. 2003); however, the amplitude of the variations is larger in the Bering Sea (Yang et al. 2020). Although such low-frequency variability could potentially arise from mechanisms related to permafrost geomorphology in colder parts of the Arctic, such as patterns of disturbance and vegetation succession associated with widespread ice-wedge degradation in northern Alaska (Lara et al. 2018), these features are not well developed on the YKD. Soil and surface moisture may become more important as temperatures increase; for example, permafrost thaw can reduce soil moisture in the rooting zone (Webb et al. 2022), and changes in seasonal precipitation patterns can alter surface moisture balances. Deepening our understanding of climate drivers of surface processes will require an investigation into long-term moisture transport and seasonal precipitation patterns in the context of NDVI and growing-season dynamics.

Evidence for an enhanced hydrological cycle in the Arctic (Bintanja 2018) and climate analysis for the YKD using ERA5 atmospheric reanalysis data indicate an increase in convective precipitation (not shown). This in addition to tundra drying trends (Webb et al. 2022) have implications for increasing the potential for tundra wildfires throughout the Arctic, and particularly the YKD. The extraordinary 2022 fire season in Alaska's southwest fire management area, which contains the YKD study region, burnt a record 1.3 million acres (1 acre = 0.4 ha), far surpassing the previous record set in 2015 by over 400 000 acres (900 000 acres burnt in 2015; Alaska Interagency Coordination Center 2022). Future research that focuses on the hydrologic cycle to examine long-term climate trends and variability will lead to a better understanding of how tundra vegetation on the YKD might be impacted as spring sea ice continues to decline and the relationship between sea ice concentration and summer temperature weakens. As spring sea ice concentration in the Bering Sea continues to decline and impact changing climate controls on Arctic tundra productivity, the question of how much longer the YKD can be classified as "Arctic" tundra will become more relevant.

b. *Length of data records and covariance*

Decadal variability of spring sea ice concentration along seasonal transition zones like the YKD can be hard to discern where there is strong interannual variability. Strong interannual variability can also obscure long-term relationships among climate data records. This study makes use of the 40-yr AVHRR NDVI record to investigate long-term and decadal

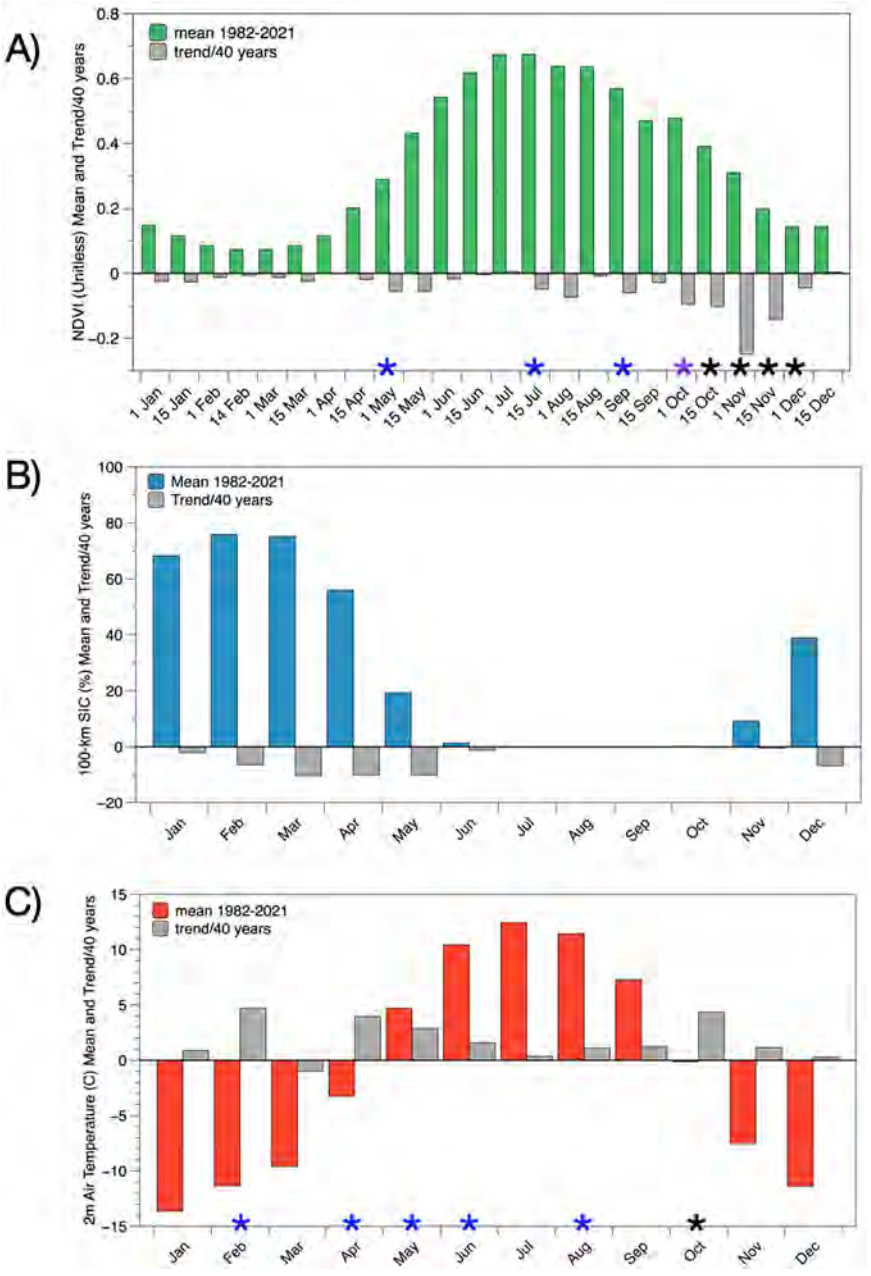

FIG. 3. Seasonality plots showing climatology (colors) and trends (gray) for (a) biweekly MaxNDVI (green; unitless), (b) monthly 100-km coastal sea ice concentration (blue; %), and (c) monthly 2-m air temperature (red; °C). Confidence of trends is indicated by asterisks at the 90% (blue), 95% (purple), and 99% (black) or greater level.

trends on the YKD. It highlights the importance of investigating climate variables together over decadal time scales to understand relationships between climate drivers and indicators. Previous research has noted decadal variability in climate variables; for example, Bhatt et al. (2017) split the time series of climate variables by noticeable trend changes in monthly summer temperature for the pan-Arctic scale. In the referenced study, sea ice decline during the spring was greater in the early part of the data record (1982–98) than in the later part (1999–2015), and summer warmth and NDVI displayed stronger positive trends in the early period than in the later period. Our study confirms that the larger pan-Arctic relationship is also valid at the regional level, but in the Bering Sea region these relationships can be confounded by large interannual variability. In a recent study by Frost et al. (2021) that focused on comparing NDVI trends from different satellite sensors with shorter data records for 2000–19,

the shortened study period did not reveal the low-frequency variability. There is some uncertainty as to the large-scale on-the-ground truth of YKD tundra variability given the differences between the Moderate Resolution Imaging Spectroradiometer (MODIS) and AVHRR TI-NDVI records; however, variability of biweekly NDVI is similar for both sensors. While newer sensors with finer spatial resolution and improved calibration such as MODIS and Visible Infrared Imaging Radiometer Suite (VIIRS) are unparalleled for observing environmental change with daily temporal resolution since 2000 and 2012, respectively, the consistent four-decade (1982–2021) AVHRR NDVI record is invaluable for revealing the ecosystem impacts of low-frequency variability in the climate system. The development of seamless data records by combining different sensors of key Arctic indicators such as biweekly NDVI is a high priority to continue monitoring activities such as the Arctic Report Card (e.g., Frost et al. 2022, 2023).

5. Conclusions

This paper provides insights into Arctic climate processes operating at regional scales over four decades during a time of rapid change. Widespread declining NDVI trends on the YKD are a striking contrast to greening trends across the circumpolar Arctic tundra; however, long-term data record analysis reveals that coherent low-frequency variability in spring sea ice concentration and the associated influence on summer temperatures can account for the negative linear trends and more recent positive NDVI trends. NDVI displays distinct decadal-scale variability that influences the interpretation of trends. Both TI-NDVI and biweekly NDVI show an increasing trend early in the record that peaked during the 1990s, followed by a steady decline until around 2010. Since 2010 there has been a sharp rise in both TI-NDVI and biweekly NDVI through 2021. The decadal-scale variations in the TI-NDVI correlate significantly with the sea ice variations and the associated summer warmth variations. While the early half of the study period shows high interannual variability and a lack of coherence among NDVI, sea ice and air temperature, since about 2005, variations of TI-NDVI, spring sea ice concentration, and summer warmth show more coherent interannual variability. Seasonality analysis for the entire record shows declining sea ice concentration in the months leading up to the growing season, followed by weakly declining trends for NDVI in all months of the growing season, despite increasing temperatures during all months of the growing season. A second key result is the relationship between sea ice concentration and summer warmth, and sea ice concentration and NDVI have strengthened since 2010. In contrast, the relationship has weakened between TI-NDVI and summer warmth, indicating that temperature may no longer be the limiting factor for Arctic tundra vegetation on the YKD. Low-frequency variability is an essential but heretofore little-discussed element of tundra vegetation dynamics, and AVHRR NDVI data, with their long period of record, are essential for observing and understanding decadal climate–vegetation relationships.

Acknowledgments. This research was supported by NASA's Arctic-Boreal Vulnerability Experiment (ABoVE) initiative under Grants 80NSSC22K1256 (author Frost) and 80NSSC22K1257 (author Bhatt). Authors Bhatt, Frost, and Hendricks acknowledge support from NASA Grant NNH16CP09C as part of the Arctic Boreal Vulnerability Experiment. The authors declare no conflicts of interest. The authors thank the editing staff of *Earth Interactions* and anonymous reviewers for their time and insightful feedback to improve the paper.

Data availability statement. All of the data used in this study are publicly available. GIMMs3g NDVI data are being archived at the NASA ABoVE Oak Ridge National Laboratory (ORNL) Distributed Active Archive Center (DAAC) (https://daac.ornl.gov/VEGETATION/guides/Global_Veg_Greenness_GIMMS_3G.html). ERA5 data are available online (https://www.ecmwf.int/en/forecasts/dataset/ecmwf-reanalysis-v5).

APPENDIX

Additional Materials

Figure A1 and Table A1 provide detailed information on the six physiographic regions of the Yukon–Kuskokwim Delta. Figure A2 shows the normalized time series for 100-km spring sea ice concentration, summer warmth index, and TI-NDVI.

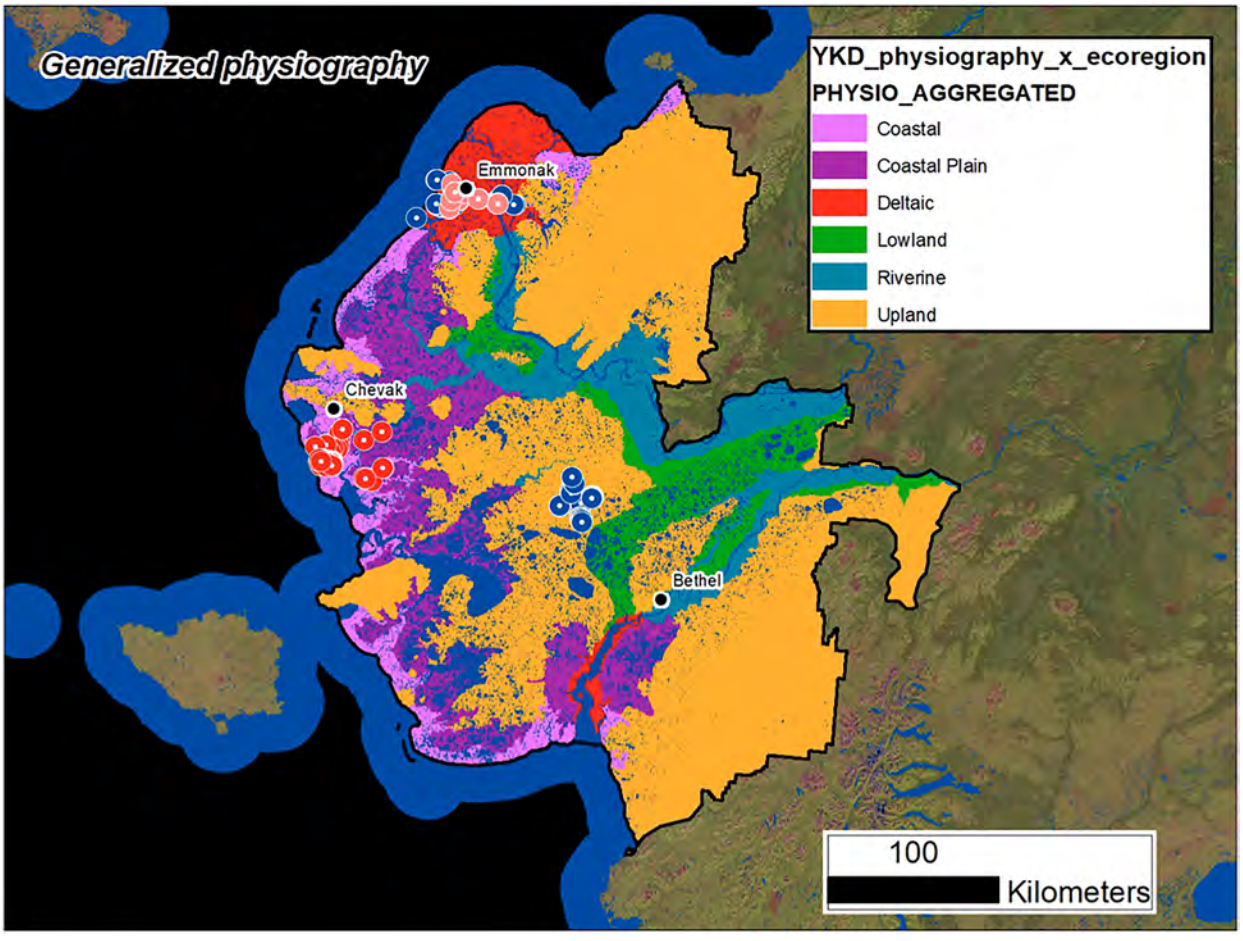

FIG. A1. Physiographic regions of the YKD. The dots represent field plots in Frost et al. (2021).

TABLE A1. Description and extent of physiographic units in the YKD study region [modified from Frost et al. (2021)].

Physiographic unit	Area (km^2)	Percent of total (%)	Description
Coastal	8167	8.5	Flat, low-lying areas near the coast, subject to saltwater inundation
Coastal plain	14 445	15.0	Flat, low-lying areas near the coast that are not regularly subject to saltwater inundation
Deltaic	5282	5.5	Modern deltas of the Yukon and Kuskokwim Rivers
Lowland	7346	7.6	Flat inland areas occupying low position in topography but not associated with floodplains
Riverine	9385	9.8	Nondeltaic floodplains that experience regular fluvial sedimentation and erosion
Upland	51 553	53.6	Rolling hills and isolated mountains; high position in local topography
Total	96 178	100.0	

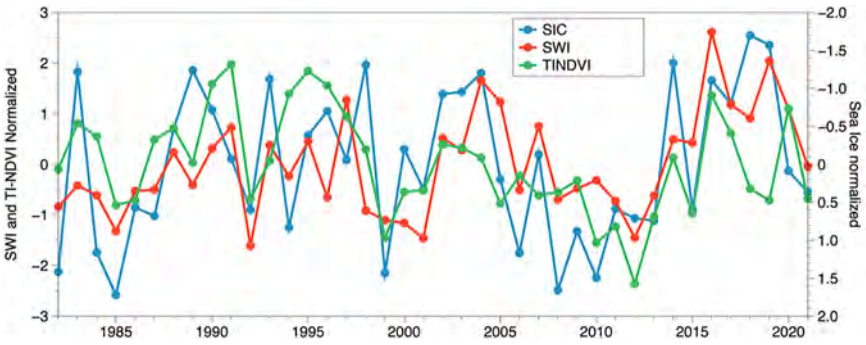

FIG. A2. Normalized time series for 100-km spring sea ice concentration (blue), summer warmth index (red), and TI-NDVI (green).

REFERENCES

Alaska Interagency Coordination Center, 2022: Welcome to the Alaska Interagency Coordination Center. Alaska Interagency Coordination Center, accessed 2 September 2022, https://fire.ak.blm.gov/.

Ballinger, T. J., and Coauthors, 2022: Arctic Report Card 2020: Surface air temperature. NOAA, 7 pp., https://doi.org/10.25923/gcw8-2z06.

Berner, L. T., and Coauthors, 2020: Summer warming explains widespread but not uniform greening in the Arctic tundra biome. *Nat. Commun.*, **11**, 4621, https://doi.org/10.1038/s41467-020-18479-5.

Bhatt, U. S., and Coauthors, 2010: Circumpolar Arctic tundra vegetation change is linked to sea ice decline. *Earth Interact.*, **14**, https://doi.org/10.1175/2010EI315.1.

——, and Coauthors, 2017: Changing seasonality of panarctic tundra vegetation in relationship to climatic variables. *Environ. Res. Lett.*, **12**, 055003, https://doi.org/10.1088/1748-9326/aa6b0b.

——, and Coauthors, 2021: Climate drivers of Arctic tundra variability and change using an indicators framework. *Environ. Res. Lett.*, **16**, 055019, https://doi.org/10.1088/1748-9326/abe676.

Bieniek, P. A., and Coauthors, 2012: Climate divisions for Alaska based on objective methods. *J. Appl. Meteor. Climatol.*, **51**, 1276–1289, https://doi.org/10.1175/JAMC-D-11-0168.1.

——, and Coauthors, 2015: Climate drivers linked to changing seasonality of Alaska coastal tundra vegetation productivity. *Earth Interact.*, **19**, https://doi.org/10.1175/EI-D-15-0013.1.

——, U. S. Bhatt, J. E. Walsh, R. Lader, B. Griffith, J. K. Roach, and R. L. Thoman, 2018: Assessment of Alaska rain-on-snow events using dynamical downscaling. *J. Appl. Meteor. Climatol.*, **57**, 1847–1863, https://doi.org/10.1175/JAMC-D-17-0276.1.

Bintanja, R., 2018: The impact of Arctic warming on increased rainfall. *Sci. Rep.*, **8**, 16001, https://doi.org/10.1038/s41598-018-34450-3.

Bjerke, J. W., S. R. Karlsen, K. A. Høgda, E. Malnes, J. U. Jepsen, S. Lovibond, D. Vikhamar-Schuler, and H. Tømmervik, 2014: Record-low primary productivity and high plant damage in the Nordic Arctic region in 2012 caused by multiple weather events and pest outbreaks. *Environ. Res. Lett.*, **9**, 084006, https://doi.org/10.1088/1748-9326/9/8/084006.

Bokhorst, S. F., J. W. Bjerke, H. Tømmervik, T. V. Callaghan, and G. K. Phoenix, 2009: Winter warming events damage sub-Arctic vegetation: Consistent evidence from an experimental manipulation and a natural event. *J. Ecol.*, **97**, 1408–1415, https://doi.org/10.1111/j.1365-2745.2009.01554.x.

Box, J. E., and Coauthors, 2019: Key indicators of Arctic climate change: 1971–2017. *Environ. Res. Lett.*, **14**, 045010, https://doi.org/10.1088/1748-9326/aafc1b.

Chapin, F. S., III, G. R. Shaver, A. E. Giblin, K. J. Nadelhoffer, and J. A. Laundre, 1995: Responses of Arctic Tundra to experimental and observed changes in climate. *Ecology*, **76**, 694–711, https://doi.org/10.2307/1939337.

Circumpolar Arctic Vegetation Map Team, 2003: Circumpolar Arctic vegetation map (1:7,500,000 scale). Conservation of Arctic Flora and Fauna (CAFF) Map No. 1. U.S. Fish and Wildlife Service, https://www.geobotany.uaf.edu/cavm/finalcavm/side1_1200x1600.jpg.

Comiso, J. C., and F. Nishio, 2008: Trends in the sea ice cover using enhanced and compatible AMSR-E, SSM/I, and SMMR data. *J. Geophys. Res.*, **113**, C02S07, https://doi.org/10.1029/2007JC004257.

Fienup-Riordan, A., 1999: Yaqulget qaillun pilartat (What the birds do): Yup'ik Eskimo understanding of geese and those who study them. *Arctic*, **52** (1), 1–22, https://doi.org/10.14430/arctic905.

Frost, G. V., R. A. Loehman, L. B. Saperstein, M. J. Macander, P. R. Nelson, D. P. Paradis, and S. M. Natali, 2020: Multi-decadal patterns of vegetation succession after tundra fire on the Yukon-Kuskokwim Delta, Alaska. *Environ. Res. Lett.*, **15**, 025003, https://doi.org/10.1088/1748-9326/ab5f49.

——, U. S. Bhatt, M. J. Macander, A. S. Hendricks, and M. T. Jorgenson, 2021: Is Alaska's Yukon–Kuskokwim Delta greening or browning? Resolving mixed signals of tundra vegetation dynamics and drivers in the maritime Arctic. *Earth Interact.*, **25**, https://doi.org/10.1175/EI-D-20-0025.1.

——, and Coauthors, 2022: Tundra greenness [in "State of the Climate in 2021"]. *Bull. Amer. Meteor. Soc.*, **103** (8), S291–S293, https://doi.org/10.1175/BAMS-D-22-0082.1.

——, and Coauthors, 2023: Tundra greenness [in "State of the Climate in 2022"]. *Bull. Amer. Meteor. Soc.*, **104** (9), S305–S308, https://doi.org/10.1175/BAMS-D-23-0079.1.

Gamon, J. A., K. F. Huemmrich, R. S. Stone, and C. E. Tweedie, 2013: Spatial and temporal variation in primary productivity (NDVI) of coastal Alaskan tundra: Decreased vegetation growth following earlier snowmelt. *Remote Sens. Environ.*, **129**, 144–153, https://doi.org/10.1016/j.rse.2012.10.030.

Gill, R. E., Jr., and C. M. Handel, 1990: The importance of subarctic intertidal habitats to shorebirds: A study of the central Yukon-Kuskokwim Delta, Alaska. *Condor*, **92**, 709–725, https://doi.org/10.2307/1368690.

Goetz, S. J., and Coauthors, 2010: Recent changes in Arctic vegetation: Satellite observations and simulation model predictions.

Eurasian Arctic Land Cover and Land Use in a Changing Climate, Springer, 9–36.

Hersbach, H., and Coauthors, 2020: The ERA5 global reanalysis. *Quart. J. Roy. Meteor. Soc.*, **146**, 1999–2049, https://doi.org/10.1002/qj.3803.

Holland, M. M., and C. M. Bitz, 2003: Polar amplification of climate change in coupled models. *Climate Dyn.*, **21**, 221–232, https://doi.org/10.1007/s00382-003-0332-6.

Jia, G. J., H. E. Epstein, and D. A. Walker, 2003: Greening of Arctic Alaska, 1981–2001. *Geophys. Res. Lett.*, **30**, 2067, https://doi.org/10.1029/2003GL018268.

Jorgenson, M. T., G. V. Frost, and D. Dissing, 2018: Drivers of landscape changes in coastal ecosystems on the Yukon-Kuskokwim Delta, Alaska. *Remote Sens.*, **10**, 1280, https://doi.org/10.3390/rs10081280.

Klein, D. R., 1966: Waterfowl in the economy of the Eskimos on the Yukon-Kuskokwim Delta, Alaska. *Arctic*, **19**, 319–336, https://doi.org/10.14430/arctic3438.

Lara, M. J., I. Nitze, G. Grosse, P. Martin, and A. D. McGuire, 2018: Reduced Arctic tundra productivity linked with landform and climate change interactions. *Sci. Rep.*, **8**, 2345, https://doi.org/10.1038/s41598-018-20692-8.

Myers-Smith, I. H., and Coauthors, 2020: Complexity revealed in the greening of the Arctic. *Nat. Climate Change*, **10**, 106–117, https://doi.org/10.1038/s41558-019-0688-1.

Myneni, R. B., C. D. Keeling, C. J. Tucker, G. Asrar, and R. R. Nemani, 1997: Increased plant growth in the northern high latitudes from 1981 to 1991. *Nature*, **386**, 698–702, https://doi.org/10.1038/386698a0.

NCEI, 2022: Climate at a glance. NOAA, accessed 12 August 2022, https://www.ncei.noaa.gov/cag/divisional/time-series.

Nowacki, G. J., P. Spencer, M. Fleming, T. Brock, and T. Jorgenson, 2003: Unified ecoregions of Alaska: 2001. USGS Open-File Rep. 2002-297, 2 pp., https://doi.org/10.3133/ofr2002297.

Park, T., and Coauthors, 2016: Changes in growing season duration and productivity of northern vegetation inferred from long-term remote sensing data. *Environ. Res. Lett.*, **11**, 084001, https://doi.org/10.1088/1748-9326/11/8/084001.

Pinzon, J. E., and C. J. Tucker, 2014: A non-stationary 1981–2012 AVHRR $NDVI_{3g}$ time series. *Remote Sens.*, **6**, 6929–6960, https://doi.org/10.3390/rs6086929.

——, E. W. Pak, C. J. Tucker, U. S. Bhatt, G. V. Frost, and M. J. Macander, 2023: Global Vegetation Greenness (NDVI) from AVHRR GIMMS-3G+, 1981–2022. ORNL DAAC, accessed 24 February 2022, https://doi.org/10.3334/ORNLDAAC/2187.

Polyakov, I. V., and Coauthors, 2003: Long-term ice variability in Arctic marginal seas. *J. Climate*, **16**, 2078–2085, https://doi.org/10.1175/1520-0442(2003)016<2078:LIVIAM>2.0.CO;2.

Raynolds, M. K., J. C. Comiso, D. A. Walker, and D. Verbyla, 2008: Relationship between satellite-derived land surface temperatures, Arctic vegetation types, and NDVI. *Remote Sens. Environ.*, **112**, 1884–1894, https://doi.org/10.1016/j.rse.2007.09.008.

Reichle, L. M., H. E. Epstein, U. S. Bhatt, M. K. Raynolds, and D. A. Walker, 2018: Spatial heterogeneity of the temporal dynamics of Arctic tundra vegetation. *Geophys. Res. Lett.*, **45**, 9206–9215, https://doi.org/10.1029/2018GL078820.

Santer, B. D., T. M. L. Wigley, J. S. Boyle, D. J. Gaffen, J. J. Hnilo, D. Nychka, D. E. Parker, and K. E. Taylor, 2000: Statistical significance of trends and trend differences in layer-average atmospheric temperature time series. *J. Geophys. Res.*, **105**, 7337–7356, https://doi.org/10.1029/1999JD901105.

Screen, J. A., and I. Simmonds, 2010: The central role of diminishing sea ice in recent Arctic temperature amplification. *Nature*, **464**, 1334–1337, https://doi.org/10.1038/nature09051.

Stroeve, J., M. M. Holland, W. Meier, T. Scambos, and M. Serreze, 2007: Arctic sea ice decline: Faster than forecast. *Geophys. Res. Lett.*, **34**, L09501, https://doi.org/10.1029/2007GL029703.

Tucker, C. J., 1977: Use of near infrared/red radiance ratios for estimating vegetation biomass and physiological status. NASA Tech. Memo. X-923-77-183, 47 pp., https://ntrs.nasa.gov/citations/19770025621.

——, J. E. Pinzon, M. E. Brown, D. A. Slayback, E. W. Pak, R. Mahoney, E. F. Vermote, and N. El Saleous, 2005: An extended AVHRR 8-km NDVI dataset compatible with MODIS and SPOT vegetation NDVI data. *Int. J. Remote Sens.*, **26**, 4485–4498, https://doi.org/10.1080/01431160500168686.

Verbyla, D., 2008: The greening and browning of Alaska based on 1982–2003 satellite data. *Global Ecol. Biogeogr.*, **17**, 547–555, https://doi.org/10.1111/j.1466-8238.2008.00396.x.

Walker, D. A., and Coauthors, 2003: Phytomass, LAI, and NDVI in northern Alaska: Relationships to summer warmth, soil pH, plant functional types, and extrapolation to the circumpolar Arctic. *J. Geophys. Res.*, **108**, 8169, https://doi.org/10.1029/2001JD000986.

——, and Coauthors, 2005: The circumpolar Arctic vegetation map. *J. Veg. Sci.*, **16**, 267–282, https://doi.org/10.1111/j.1654-1103.2005.tb02365.x.

Webb, E. E., A. K. Liljedahl, J. A. Cordeiro, M. M. Loranty, C. Witharana, and J. W. Lichstein, 2022: Permafrost thaw drives surface water decline across lake-rich regions of the Arctic. *Nat. Climate Change*, **12**, 841–846, https://doi.org/10.1038/s41558-022-01455-w.

White, J. H. R., J. E. Walsh, and R. L. Thoman Jr., 2021: Using Bayesian statistics to detect trends in Alaskan precipitation. *Int. J. Climatol.*, **41**, 2045–2059, https://doi.org/10.1002/joc.6946.

Yang, X.-Y., G. Wang, and N. Keenlyside, 2020: The Arctic sea ice extent change connected to Pacific decadal variability. *Cryosphere*, **14**, 693–708, https://doi.org/10.5194/tc-14-693-2020.